Theoretical analysis of bimetallic nanorod dimer biosensors for label-free molecule detection

Avijit Das, and Muhammad Anisuzzaman Talukder

Citation: AIP Advances **8**, 025302 (2018); doi: 10.1063/1.5010902
View online: https://doi.org/10.1063/1.5010902
View Table of Contents: http://aip.scitation.org/toc/adv/8/2
Published by the American Institute of Physics

Theoretical analysis of bimetallic nanorod dimer biosensors for label-free molecule detection

Avijit Das and Muhammad Anisuzzaman Talukder[a]
Department of Electrical and Electronic Engineering, Bangladesh University of Engineering and Technology, Dhaka 1205, Bangladesh

(Received 27 October 2017; accepted 25 January 2018; published online 5 February 2018)

In this work, we theoretically analyze a gold (Au) core within silver (Ag) shell (Au@Ag) nanorod dimer biosensor for label-free molecule detection. The incident light on an Au@Ag nanorod strongly couples to localized surface plasmon modes, especially around the tip region. The field enhancement around the tip of a nanorod or between the tips of two longitudinally aligned nanorods as in a dimer can be exploited for sensitive detection of biomolecules. We derive analytical expressions for the interactions of an Au@Ag nanorod dimer with the incident light. We also study the detail dynamics of an Au@Ag nanorod dimer with the incident light computationally using finite difference time domain (FDTD) technique when core-shell ratio, relative position of the nanorods, and angle of incidence of light change. We find that the results obtained using the developed analytical model match well with that obtained using FDTD simulations. Additionally, we investigate the sensitivity of the Au@Ag nanorod dimer, i.e., shift in the resonance wavelength, when a target biomolecule such as lysozyme (Lys), human serum albumin (HSA), anti-biotin (Abn), human catalase (CAT), and human fibrinogen (Fb) protein molecules are attached to the tips of the nanorods. https://doi.org/10.1063/1.5010902

I. INTRODUCTION

Last few decades have witnessed an increasing research interest in noble metal nanoparticles—especially gold (Au)[1,2] and silver (Ag)[3,4] nanoparticles—due to their interesting optical properties. The strong localized surface plasmon resonance (LSPR) observed in Au and Ag nanoparticles is being exploited in many applications including optical microscopy and spectroscopy, nanophotonic devices, chemical and biochemical sensing, medical diagnostics and therapeutics, and optical waveguides.[5–8] LSPR in metal nanoparticles can be tuned over a broad range by using different compositions, sizes, and shapes of materials. LSPR also sensitively depends on the local dielectric environment surrounding the nanoparticles. When a biomolecule is attached to a nanoparticle, the local dielectric environment surrounding the nanoparticle changes. The change in the dielectric environment results in a shift in the peak LSPR wavelength, which is often termed as "LSPR shift." The LSPR shift due to the presence of a biomolecule can be measured to detect the biomolecule.[9]

In a typical LSPR-based biosensor, target biomolecules must be attached to the sensing platform, e.g., nanoparticles. Therefore, ligands are used to functionalize the surface of nanoparticles to recognize and selectively attach target biomolecules. The presence of the biomolecule in the surrounding changes the refractive index of the local medium, which leads to a significant shift in LSPR wavelengths, providing a sensing platform for label-free single biomolecules. Such refractive index-based sensitivity of biosensors highly depends on the frequency-dependent dielectric function of materials. For instance, Ag nanoparticles produce more polarized charges and less plasmonic damping compared to Au nanoparticles as Ag has a greater real part and a smaller imaginary part of dielectric

[a]anis@eee.buet.ac.bd

function than that of Au. Therefore, biosensors based on Ag nanoparticles are approximately twice more sensitive than that based on Au nanoparticles.[10] However, Ag-based sensors are not preferred due to their chemical instability and toxicity. By contrast, Au nanoparticles have good biocompatibility and chemical stability. However, both chemical stability and high sensitivity can be achieved in Au-core within Ag-shell (Au@Ag) structures.[11,12] Au@Ag nanospheres have already been used for biosensing, and found to be chemically more stable than bare Ag nanospheres and more sensitive than bare Au nanospheres.[13] Although, in principle, nanostructures with Ag-core within Au-shell (Ag@Au) will have similar desirable characteristics of a biosensor, the fabrication and control of shape and size of Ag@Au nanostructures are still too challenging.[11,14,15]

A different shape of Au@Ag nanoparticles, i.e., nanorods, can provide greater sensitivity than Au@Ag nanospheres due to local field enhancement at the tips. Additionally, significant field enhancement can be achieved if two nanorod monomers are longitudinally aligned with a small gap between their tips. Therefore, the sensitivity of detection of biomolecules can be increased significantly by using the longitudinally aligned coupled monomers, i.e., a dimer, with the target biomolecule placed in the gap region between the tips. Recently, a proof-of-concept demonstration of field enhancement due to the excitation of plasmonic modes in an Au@Ag nanorod dimer has been reported.[16]

The interactions of the incident light with sub-wavelength dimensional metal nanoparticles and excitation of plasmonic modes are complex physics. It is important to theoretically model the dynamics for an in-depth understanding so that plasmonic properties of nanoparticles can be exploited and optimized for sensing of biomolecules.[17] Gold nanorods have been extensively studied to understand the coupling of incident light to plasmonic modes and the change in plasmonic resonances when protein molecules attach to them.[17–19] The interaction of incident light with single nanorod homodimers has also been studied theoretically, including the change in LSPR due to the angle between excitation polarization and the dimer orientation.[20,21] Recently, localized field enhancement due to plasmonic mode excitation has been studied in Au-Ag nanorod heterodimers.[22] However, a detail theoretical analysis of Au@Ag nanorod dimer sensors including understanding of complex physics when biomolecules attach to the tips is still lacking.

In this work, we analytically and computationally investigate the plasmonic properties of Au@Ag nanorod dimers so that sensitivity can be optimized for label-free biomolecule detection. We derive analytical expressions to calculate the absorption cross-sections of nanorod dimers for transverse magnetic (TM)- and transverse electric (TE)-polarized incident light. We also calculate the detail dynamics of Au@Ag nanorod dimers for broadband incident light by computationally solving Maxwell's equations using finite difference time domain (FDTD) technique when the core-shell ratio, relative position of the nanorods, and the angle of incidence of light vary. We find that the results obtained using the developed analytical model match well with that obtained using FDTD simulations. Furthermore, we investigate the sensitivity of Au@Ag nanorod dimers for single biomolecule detection for lysozyme (Lys), human serum albumin (HSA), anti-biotin (Abn), human catalase (CAT), and human fibrinogen (Fb) protein molecules.

II. BIMETALLIC NANOROD DIMER STRUCTURE

In Fig. 1, we show a schematic illustration of an Au@Ag nanorod dimer. In an Au@Ag nanorod, an Au nanorod core is coated by an Ag shell layer. In this work, the Au@Ag nanorod has a tip-to-tip length of 33 nm and a diameter of 11 nm. Both ends of the nanorod are hemispherically capped with a radius of 5.5 nm. When two such Au@Ag nanorods are placed on a SiO_2 substrate in a longitudinal

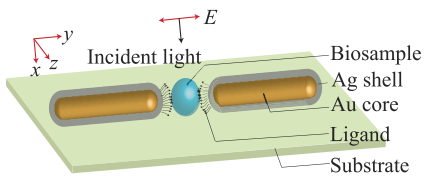

FIG. 1. Schematic illustration of Au@Ag nanorod dimer-based sensor for biomolecule detection.

TABLE I. Key parameter values of different protein molecules.

Protein	Shape	Dimension (nm)			Mass (kDa)	Refractive Index
		Major axis	Minor axis-1	Minor axis-2		
Lys	Ellipsoid	4.5	1.8	1.8	14.3	1.495
HSA	Ellipsoid	7.5	6.5	4	66.4	1.445
Abn	Ellipsoid	7.4	7.2	7.2	150	1.45
CAT	Ellipsoid	9.7	9.2	6.7	230	1.465
Fb	Elongated ellipsoid	46	6	3	390	1.39

TABLE II. Refractive indices of ligands.

Ligand	Refractive Index
Biotin	1.455
Bilirubin	1.460
Polyethylene glycol	1.457

alignment, we have a bimetallic dimer structure. A small gap of ~10 nm between the tips of nanorods is kept to probe the presence of biomolecules. It has been reported that when biomolecules are brought in the proximity of functionalized nanorods, ~65% of them attach to the tip and the rest to the side.[18] Therefore, in this work, we assume that the Au@Ag nanorods are functionalized at the tip with a 0.5-nm-layer of ligands or conjugating materials so that biomolecules are attached to the tips. As a result, essentially, biomolecules will be located in the gap between the two nanorods of the dimer. In practice, Au@Ag nanorods can be functionalized using a procedure described in Ref. 18. For example, to functionalize the tips with biotin conjugate material, first the nanorods are incubated in 2 mM cetyltrimethylammonium bromide and 2 μM thiolated biotin solution, and then flushed with phosphate buffer saline.

To investigate the performance of Au@Ag nanorod dimer biosensors in the presence of a biomolecule, we use a number of proteins as target molecules, e.g., Lys, HSA, Abn, CAT, and Fb. We note that these proteins are used as biomarkers in early detection of many severe diseases, e.g., rheumatoid arthritis, Alzheimer's disease, coronary artery disease, and pancreatic and lung cancers.[23–25] For early detection, often the target biomolecule count is extremely low so that a highly sensitive sensor, if possible, with a capacity of single molecule detection is necessary. The target molecules may also vary significantly in their physical characteristics such as size, shape and weight, and in their optical characteristics such as refractive index, which may affect the sensitivity of the sensor. The characteristic parameter values of the target biomolecules considered in this work are obtained from experimental reports[18,26–29] and are given in Table I.

Target biomolecules will need appropriate ligands or conjugate materials to make bonds and attach to the sensor platform. Thiolated biotin is often used as a conjugating material to capture a number of biomolecules, including Lys, Abn, and Fb that have been analyzed in this manuscript.[30] Bilirubin is used as a conjugate material to capture HSA and polyethylene glycol is used as a conjugate material to capture CAT.[31,32] The refractive indices of the ligands are obtained from Refs. 33–35 and given in Table II. We note that since we use only a 0.5-nm-thick conjugate material layer at the nanorod tip and the conjugate materials have almost equal refractive indices, the choice of conjugate materials does not have noticeable effect on the LSPR shifts of the nanorod dimer biosensor. We assume water as the buffer medium. Therefore, the dimer biosensor system is submerged in water.

III. ANALYTICAL MODELING

In this work, we develop a dipolar model of plasmonic behaviors of bimetallic nanorod dimers. Since the nanorods are much smaller than the wavelength of the absorbed light, they can be considered

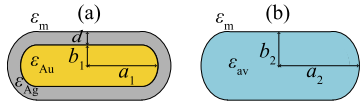

FIG. 2. (a) Au core nanorod with a semimajor axis of a_1, semiminor axis of b_1, and dielectric function of ε_{Au}. Au core is covered by an Ag layer with a thickness of d and dielectric function of ε_{Ag}. The surrounding medium has a dielectric function of ε_m. (b) Equivalent homogeneous nanorod with a semimajor axis of a_2, semiminor axis of b_2, and average dielectric function of ε_{av}.

as dipoles,[36] and the dimers can be modeled as the electrostatic interaction between two electric dipoles situated at the centers of the two nanorods. The electric dipole moments of Au@Ag nanorods will sensitively depend on the polarizability, and hence, on the average equivalent dielectric function of the nanorods. In this work, we derive expressions for absorption cross-sections of Au@Ag nanorod monomers and dimers that can be used to understand the interactions of Au@Ag nanorod monomers and dimers with the incident light.

A. Au@Ag nanorod monomer

In Fig. 2(a), we show an Au@Ag nanorod monomer that has an Au core with semimajor axis of a_1 and semiminor axis of b_1, and Ag coating layer of thickness d on the Au core. The dielectric functions of Au, Ag, and the surrounding medium are represented by ε_{Au}, ε_{Ag}, and ε_m, respectively. Optically, the bimetallic structure in a homogeneous equivalent medium can be replaced by an average dielectric function using dipole equivalence principle.[37] Figure 2(b) shows the homogeneous equivalent nanorod with semimajor axis of a_2, semiminor axis of b_2, and average dielectric function of ε_{av}. We assume that the equivalent nanorod has the same overall dimensions, i.e., $a_2 = a_1 + d$ and $b_2 = b_1 + d$. The optical properties of the equivalent nanorod are attributed to ε_{av}. Therefore, using dipole equivalency, we derive an analytical expression to calculate the average dielectric function of an Au@Ag nanorod monomer as given by

$$\varepsilon_{av} = \varepsilon_{Ag}\left[1 + \frac{f\alpha_s}{1 - f\alpha_s P_{L,T}}\right], \tag{1}$$

where f is the volume fraction of Au in an Au@Ag nanorod and α_s is the polarizability of the Au core. The parameter $P_{L,T}$ is the depolarization factor of the Au@Ag nanorod that depends on the overall dimensions a_2 and b_2.[38] The subscripts "L" and "T" represent the longitudinal and transverse modes, which are excited due to TM- and TE-polarized incident light, respectively.

We have calculated ε_{av} for an Au@Ag nanorod using the derived expression in Eq. (1). In Fig. 3, we present the real (ε_1) and imaginary (ε_2) parts of ε_{av} for different Ag shell thicknesses. We assume that $a_2 = 16.5$ nm and $b_2 = 5.5$ nm. We vary d from 0 to 3 nm, where $d = 0$ represents a bare Au nanorod. We keep $d \lesssim 3$ nm, because an Au@Ag nanorod is susceptible to physical deformation if the Ag shell occupies $\gtrsim 50\%$ of the volume fraction.[39] In Fig. 3(a), we show that ε_1 gradually increases in the wavelength range from 250 nm to 340 nm, while gradually decreases in the wavelength range from 350 nm to 650 nm when d increases. The greater or smaller value of ε_1 means more or less

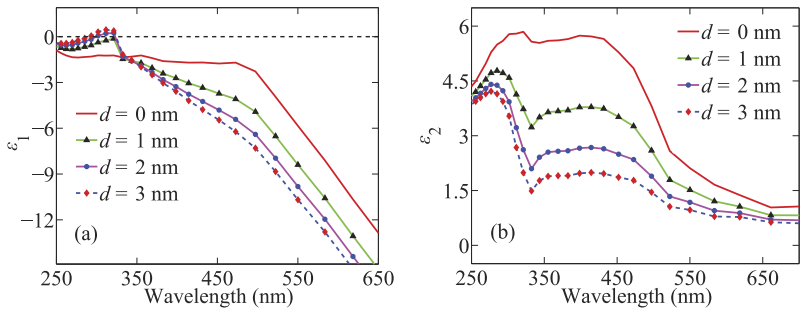

FIG. 3. (a) Real (ε_1) and (b) imaginary (ε_2) parts of the dielectric function of Au@Ag nanorods for different Ag shell thicknesses d.

polarized charges in the nanorod when light is incident. Meanwhile, ε_2 gradually decreases in the wavelength range from 250 nm to 650 nm as d increases as shown in Fig. 3(b). The greater or smaller value of ε_2 means more or less damping of the excited plasmonic modes by the incident light.

Now, an expression for the average equivalent polarizability of the Au@Ag nanorod for longitudinal and transverse plasmon modes that are excited by TM- and TE-polarized incident light, respectively, can be obtained using the derived expression of ε_{av}. In quasi-static regime, the equivalent polarizabilities α_{TM} and α_{TE} for TM- and TE-polarized incident light can be written according to Clausius-Mossotti equation as[40]

$$\alpha_{TM} = \frac{4\pi a_2 {b_2}^2}{3} \frac{\varepsilon_{av} - \varepsilon_m}{\varepsilon_m + P_L(\varepsilon_{av} - \varepsilon_m)}, \tag{2a}$$

$$\alpha_{TE} = \frac{4\pi a_2 {b_2}^2}{3} \frac{\varepsilon_{av} - \varepsilon_m}{\varepsilon_m + P_T(\varepsilon_{av} - \varepsilon_m)}. \tag{2b}$$

Equation (2) can be considered as the basis for calculating the absorption cross-section (σ) of a nanorod. The absorption cross-sections of a nanorod depends on the imaginary parts of α_{TM} and α_{TE}, and can be written as[41]

$$\sigma_{TM} = \left(\frac{2\pi}{\lambda}\right) \mathrm{Im}(\alpha_{TM}), \tag{3a}$$

$$\sigma_{TE} = \left(\frac{2\pi}{\lambda}\right) \mathrm{Im}(\alpha_{TE}), \tag{3b}$$

where λ is the wavelength of the incident light.

B. Au@Ag nanorod dimer

In Fig. 4, we show an Au@Ag nanorod dimer, where each of the nanorods is represented by its average dielectric function ε_{av}. The longitudinal direction of the nanorods is aligned with the y-axis of the coordinate system and the transverse direction is aligned with the z-axis. Therefore, the angle between the longitudinal directions of the nanorods is 180°. Using the coordinate system of Fig. 4, the electric dipole moment of each nanorod under an externally applied electric field $\mathbf{E}_0$ can be calculated by[36]

$$\mathbf{p}_i = \varepsilon_0 \varepsilon_m \alpha_i \mathbf{E}_i, \tag{4}$$

where $\mathbf{p_i}$ is the electric dipole moment of the nanorod, $\mathbf{E_i}$ is the total electric field acting on the nanorod, and ε_0 is the vacuum permittivity. The subscript i = 1, 2 represents either of the two nanorods. The electric field $\mathbf{E_i}$ includes the external field $\mathbf{E_0}$ and the field caused by the electric dipole moment of the other nanorod. When i = 1, the total electric field can be written as[36]

$$\mathbf{E}_1 = \mathbf{E}_0 + \gamma \frac{3(\mathbf{p}_2.\hat{\mathbf{e}}_{21})\hat{\mathbf{e}}_{21} - \mathbf{p}_2}{4\pi\varepsilon_0\varepsilon_m r^3}, \tag{5}$$

where r is the center-to-center distance between the nanorods, $\hat{\mathbf{e}}_{21}$ is the unit vector pointing from the center of the second nanorod to the center of the first nanorod, and γ is a coefficient introduced to take into account the bonding and antibonding plasmon resonances in the nanorod dimer. From Fig. 4, $r = 2a_2 + s$, where s is the gap between the tips of the nanorods.

In the defined geometry and coordinate system of Fig. 1, TM-polarized $\mathbf{E_0}$ will have electric field components in the x-y plane, while TE-polarized $\mathbf{E_0}$ will have field components in the x-z plane. For each polarization plane of $\mathbf{E_0}$, we find expressions for $\mathbf{p_1}$ and $\mathbf{p_2}$, and $\mathbf{E_1}$, and $\mathbf{E_2}$ for the nanorods following Eqs. (4) and (5). We solve the coupled equations for $\mathbf{p_1}$, $\mathbf{p_2}$, $\mathbf{E_1}$, and $\mathbf{E_2}$ for TM- and TE-polarized incident light. Then we add $\mathbf{p_1}$ and $\mathbf{p_2}$ along each polarization plane of $\mathbf{E_0}$ to calculate

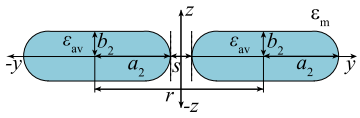

FIG. 4. Schematic illustration of an Au@Ag nanorod dimer with average dielectric function ε_{av}.

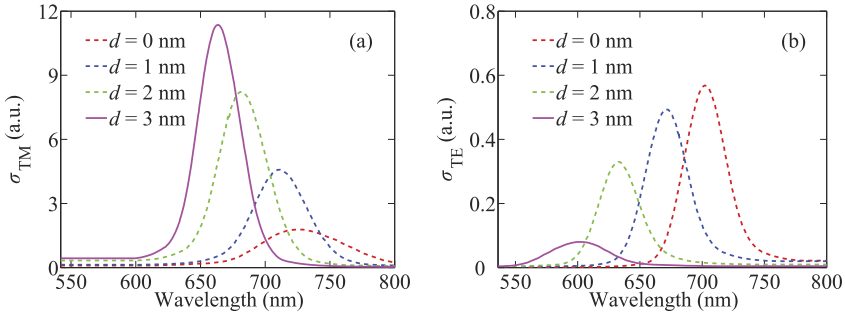

FIG. 5. Absorption cross-sections of the Au@Ag nanorod dimer to the incident (a) TM- and (b) TE-polarized incident light for different Ag shell thicknesses d calculated using the derived expressions in Eq. (7).

the total dipole moment of the dimer for each polarization. For TM- and TE-polarized incident light, we derive expressions for electric dipole moments of the dimer structure as

$$\mathbf{p}_{\mathrm{TM}} = \frac{2\varepsilon_0\varepsilon_{\mathrm{m}}\alpha_{\mathrm{TM}}\left[1-\left(\alpha_{\mathrm{TM}}\gamma_{\mathrm{B}}/4\pi r^3\right)\right]}{1+\left(\alpha_{\mathrm{TM}}{}^2\gamma_{\mathrm{B}}{}^2/8\pi^2 r^6\right)}\mathbf{E}_{0xy}, \tag{6a}$$

$$\mathbf{p}_{\mathrm{TE}} = \frac{2\varepsilon_0\varepsilon_{\mathrm{m}}\alpha_{\mathrm{TE}}\left[1+\left(\alpha_{\mathrm{TE}}\gamma_{\mathrm{A}}/4\pi r^3\right)\right]}{1+\left(\alpha_{\mathrm{TE}}{}^2\gamma_{\mathrm{A}}{}^2/8\pi^2 r^6\right)}\mathbf{E}_{0xz}. \tag{6b}$$

In Eq. (6), $\mathbf{p_{TM}}$ and $\mathbf{p_{TE}}$ stand for electric dipole moments of the Au@Ag dimer for TM- and TE-polarized incident light, respectively. We note that the TM-polarized incident light creates bonding plasmon modes, while the TE-polarized incident light creates antibonding plasmon modes in the dimer structure. The bonding and antibonding modes are considered in Eq. (6) with modifying coefficients γ_{B} and γ_{A}, respectively. The values of γ_{B} and γ_{A} that give us the best fit to the experimental results of Ref. 14 are 3.3 and 0.3, respectively.

Now, we derive expressions for polarizabilities of the Au@Ag nanorod dimer for TM- and TE-polarized incident light using Eq. (4), and use the expressions of polarizabilities to derive expressions for the absorption cross-sections using Eq. (3). The derived expressions for the absorption cross-sections are

$$\sigma_{\mathrm{TM}} = \frac{2\pi}{\lambda}\mathrm{Im}\left[\frac{2\alpha_{\mathrm{TM}}\left[1-\left(\alpha_{\mathrm{TM}}\gamma_{\mathrm{B}}/4\pi r^3\right)\right]}{1+\left(\alpha_{\mathrm{TM}}{}^2\gamma_{\mathrm{B}}{}^2/8\pi^2 r^6\right)}\right], \tag{7a}$$

$$\sigma_{\mathrm{TE}} = \frac{2\pi}{\lambda}\mathrm{Im}\left[\frac{2\alpha_{\mathrm{TE}}\left[1+\left(\alpha_{\mathrm{TE}}\gamma_{\mathrm{A}}/4\pi r^3\right)\right]}{1+\left(\alpha_{\mathrm{TE}}{}^2\gamma_{\mathrm{A}}{}^2/8\pi^2 r^6\right)}\right], \tag{7b}$$

where σ_{TM} and σ_{TE} are the absorption cross-sections of the nanorod dimer for TM- and TE-polarized incident light, respectively.

We calculate σ_{TM} and σ_{TE} of the dimer for different Ag shell thicknesses using the derived expressions in Eq. (7). The results are given in Fig. 5. We vary d from 0 to 3 nm keeping a_2 = 16.5 nm and b_2 = 5.5 nm. In Fig. 5(a), we observe that σ_{TM} increases as d increases. By contrast, in Fig. 5(b), we observe that σ_{TE} decreases as d increases. We note that σ_{TE} is much smaller than σ_{TM}. Therefore, the LSPR mode in an Au@Ag nanorod dimer with TM-polarized incident light is much stronger than that with TE-polarized incident light. Hence, the sensitivity of the Au@Ag nanorod dimer will be much greater for a change of refractive index in the surrounding medium when TM-polarized light is incident compared to when TE-polarized light is incident.

IV. FDTD SIMULATIONS

To calculate the detail LSPR dynamics of an Au@Ag nanorod dimer when broadband light with wavelengths in the visible spectral range is incident, we solve Maxwell's electromagnetic equations using a three-dimensional full-field FDTD technique. In particular, we study the change in interactions

when the volume fraction of Au core and Ag shell, the relative position of the nanorods in the dimer, and the angle of incident light vary. We also study the change in LSPR when biomolecules are attached to the tips of the nanorods in the gap region so that the sensitivity performance of Au@Ag nanorod dimers as biosensors can be understood.

A. Setup

In our simulation setup, we use a computational volume of 200 nm × 200 nm × 200 nm that contains the biosensor system. We apply perfectly matched layer boundary condition in all directions. We use a uniform mesh size of 0.5 nm within a region that encompasses the dimer structure and a uniform mesh size of 1 nm further away from the dimer. We use frequency-dependent complex refractive indices for Au and Ag according to Johnson and Christy.[42] We use water as the buffer medium and SiO_2 as the substrate with constant refractive indices of 1.33 and 1.45, respectively. For modeling different biomolecules, we consider their characteristic differences in size, shape, and refractive index according to Table I.

In this work, we study the response of an Au@Ag nanorod dimer to both TM- and TE-polarized light. The incident light is a broadband pulse with wavelengths from 400 nm to 900 nm. After solving the Maxwell's equations using FDTD technique, we calculate the absorption using[43]

$$P_{\text{abs}} = \frac{1}{2} \times \varepsilon_0 \times \omega \times \text{Im}(\varepsilon_{\text{av}})|\mathbf{E}|^2, \tag{8}$$

where ω is the frequency of incident light. We find the total absorption by integrating Eq. (8) over the spatial dimensions of the Au@Ag nanorod structure. We calculate the absorption cross-section by taking the ratio of total absorption to total incident source intensity. The LSPR shift is calculated as the difference of peak wavelengths between the absorption cross-sections with and without the biomolecules.

B. Results

1. Core-shell ratio

We calculate absorption cross-sections of Au@Ag nanorod dimers using FDTD simulations for TM- and TE-polarized incident light for different ratios of Au core and Ag shell. We vary Ag shell thickness d from 1 to 3 nm while keeping the total dimensions fixed, i.e., $a_2 = 16.5$ nm and $b_2 = 5.5$ nm. Figure 6 presents the absorption spectra of the Au@Ag nanorod dimer for TM- and TE-polarized incident light for different shell thicknesses d. We note that σ_{TM} increases as d increases as shown in Fig. 6(a). By contrast, σ_{TE} decreases as d increases as shown in Fig. 6(b). We also note that $\sigma_{\text{TM}} \ll \sigma_{\text{TE}}$. The relationships between σ_{TM} and d and between σ_{TE} and d obtained using FDTD simulations match well with those calculated using the developed analytical expressions presented in Fig. 5. We note that we observe some weak multipole plasmon resonances in σ_{TE} profiles obtained using FDTD simulations, which are not observed in the σ_{TE} profiles calculated using the developed analytical expression. We attribute this discrepancy to the inherent dipolar assumption of the nanorods adopted in the derivation of the analytical expressions.[36]

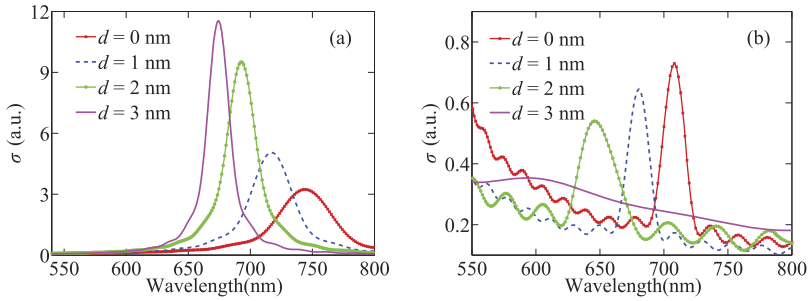

FIG. 6. Absorption cross-sections of the Au@Ag nanorod dimer to the incident (a) TM- and (b) TE-polarized incident light for different Ag shell thicknesses d calculated using FDTD technique.

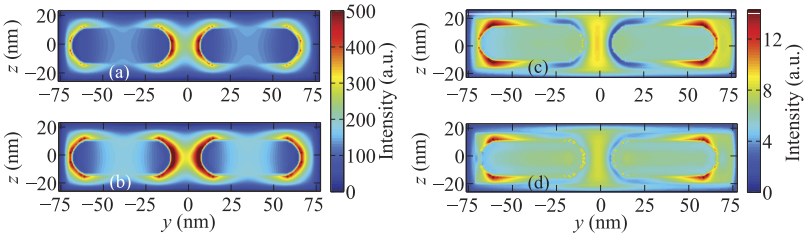

FIG. 7. Electric field profiles (|E|) of the nanorod dimer for (a) TM-polarized incident light at 710 nm with d = 1 nm, (b) TM-polarized incident light at 670 nm with d = 3 nm, (c) TE-polarized incident light at 663 nm with d = 1 nm, and (d) TE-polarized incident light at 600 nm with d = 3 nm.

In Fig. 7, we show the electric field profiles in the Au@Ag nanorod dimer for TM- and TE-polarized incident light at different resonant wavelengths. In Figs. 7(a) and 7(b), we note strong coupling of TM-polarized incident light to plasmonic modes at a resonant wavelength of 710 nm for d = 1 nm and at a resonant wavelength of 670 nm for d = 3 nm, respectively. By contrast, in Figs. 7(c) and 7(d), we note weak coupling of TE-polarized incident light to plasmonic modes at a resonant wavelength of 663 nm for d = 1 nm and at a resonant wavelength of 600 nm for d = 3 nm, respectively.

We investigate the shift in LSPR of an Au@Ag nanorod dimer structure when a CAT molecule is placed in the gap between the nanorods and the structure is illuminated by TM-polarized light. To compare the performance, we also calculate the LSPR shifts when the Au@Ag nanorod dimer is replaced by an Au@Ag nanosphere dimer and an Au@Ag nanorod monomer. Figure 8 shows the LSPR shifts for different Ag shell thicknesses. We note that the nanospheres have a radius equal to the radius of the nanorods in the transverse direction. We find that the Au@Ag nanorod dimer shows ~179% greater LSPR shift than that of an Au@Ag nanosphere dimer and ~112% greater LSPR shift than that of an Au@Ag nanorod monomer. In each case, the LSPR shift increases as the Ag shell thickness increases.

2. Nanorod positions

We study the interactions of the Au@Ag nanorod dimer with the incident light when the relative position between the two nanorods in a dimer varies as schematically shown in Fig. 9. In particular, we vary the angle θ between the longitudinal axes of the nanorods while keeping the dimensions of the nanorods fixed with a_1 = 14.5 nm, b_1 = 3.5 nm, and d = 2 nm. We also keep the spacing between the tips of the nanorods fixed at 10 nm. In each case, the incident light is normally incident, i.e., $\psi = 0°$. In Fig. 10, we show the absorption cross-sections for TM- and TE-polarized incident light for different values of θ. In Fig. 10(a), optical absorption increases for TM-polarized incident light as θ increases, while, in Fig. 10(b), optical absorption decreases for TE-polarized incident light as θ increases. Plasmonic modes are excited by TM-polarized incident light in the longitudinal direction,

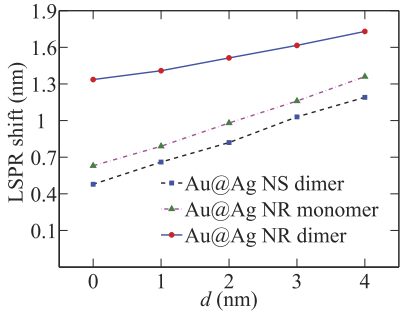

FIG. 8. LSPR shifts of an Au@Ag nanosphere (NS) dimer, an Au@Ag nanorod (NR) monomer, and an Au@Ag NR dimer when a CAT molecule is attached for different shell thicknesses d.

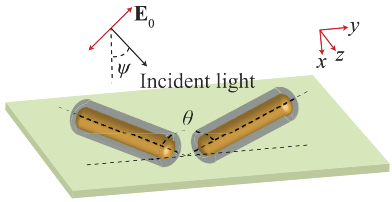

FIG. 9. Schematic illustration of an Au@Ag nanorod dimer with an angle θ between the longitudinal axes of the nanorods and an angle of incidence ψ for light.

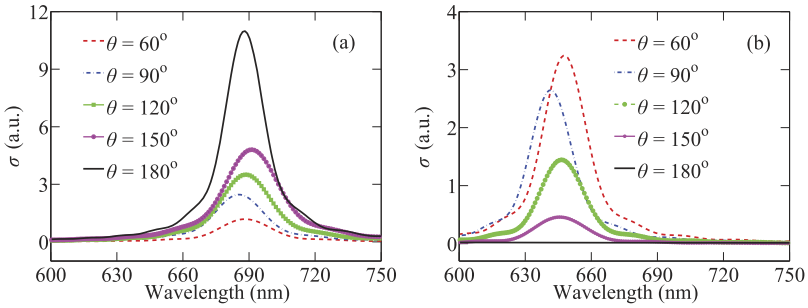

FIG. 10. Absorption cross-sections of the Au@Ag nanorod dimer to the incident (a) TM- and (b) TE-polarized light with different angles between the longitudinal axes of the nanorods.

which is maximum at $\theta = 180°$. By contrast, plasmonic modes are excited by TE-polarized incident light in the transverse direction, which is minimum at $\theta = 180°$.

Figure 11 shows the electric field profiles for TM- and TE-polarized incident light when $\theta = 60°$ and 120°. We note stronger coupling of the TM-polarized incident light to plasmonic modes at 685 nm when $\theta = 120°$ than that when $\theta = 60°$. By contrast, we find stronger coupling of the TE-polarized incident light to plasmonic modes at 647 nm when $\theta = 60°$ than that when $\theta = 120°$. We note that the field intensity is much stronger between the tips of nanorods for TM-polarized incident light than that for TE-polarized incident light.

We note that the 10-nm-gap between the nanorods is small enough for the nanorods in the dimer to interact and increase the confinement of the incident electric field in the gap region. On the contrary, the 10-nm-gap between the nanorods is large enough to accommodate a single molecule of many biological samples, e.g., a single molecule of Lys, HSA, Abn, and CAT. We note that the interaction between the nanorods and hence the sensitivity of the sensor will depend on the gap between the nanorods. If the gap is greater than 10 nm, the interaction between the nanorods will decrease and the sensitivity will decrease as well.

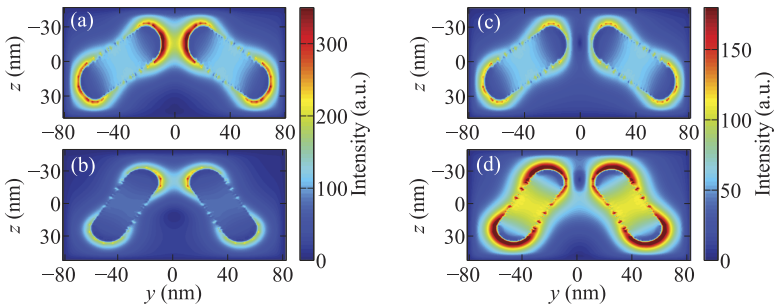

FIG. 11. Electric field profiles ($|E|$) of the Au@Ag nanorod dimer for (a) TM-polarized incident light at 685 nm when $\theta = 120°$, (b) TM-polarized incident light at 685 nm when $\theta = 60°$, (c) TE-polarized incident light at 647 nm when $\theta = 120°$, and (d) TE-polarized incident light at 647 nm when $\theta = 60°$.

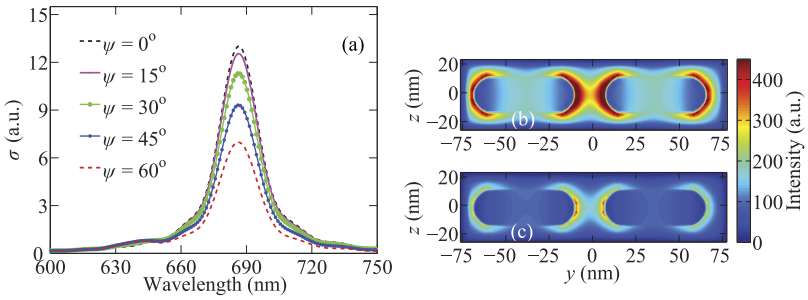

FIG. 12. (a) Absorption cross-sections of the Au@Ag nanorod dimer to the TM-polarized incident light for different incident angles ψ. Electric field profiles ($|E|$) of the nanorod dimer for TM-polarized incident light at 685 nm when (b) $\psi = 0°$ and (c) $\psi = 60°$.

3. Incidence angle of light

We study the interactions of the Au@Ag nanorod dimer with the incident light when the incidence angle varies as schematically shown in Fig. 9. We vary the incidence angle ψ while keeping the dimensions of the nanorods fixed with $a_1 = 14.5$ nm, $b_1 = 3.5$ nm, and $d = 2$ nm. In each case, the longitudinal axes of the nanorods are aligned, i.e., $\theta = 180°$. We present results only for TM-polarized incident light as the absorption does not change much with the change of ψ for TE-polarized incident light. In Fig. 12(a), we show that the optical absorption is maximum when $\psi = 0°$ and gradually decreases as ψ increases. We note that the TM-polarized incident light produces plasmon resonance at 685 nm irrespective of the value of ψ. In Figs. 12(b) and 12(c), we present the electric field profiles when $\psi = 0°$ and 60°, respectively. We note that the TM-polarized incident light strongly couples to plasmon modes and produces greater electric field intensity when $\psi = 0°$ than that when $\psi = 60°$.

4. Biomolecule detection

To understand the response of an Au@Ag nanorod dimer to the incident light in the presence of a biomolecule, we calculate the LSPR shifts when protein molecules are attached between the tips of the nanorods. The results are given in Fig. 13. In particular, we calculate LSPR shifts when Lys, HSA, Abn, CAT, and Fb molecules are attached to the tips of the Au@Ag nanorod dimer. The target biomolecules vary in size and refractive index as given in Table I. We assume that the dimer structure has dimensions $a_1 = 14.5$ nm, $b_1 = 3.5$ nm, and $d = 2$ nm. We find that the LSPR shifts are sensitive to the target biomolecules due to their varying physical dimensions and refractive indices.

In Fig. 13, we present LSPR shifts when the biomolecules have their major axis aligned with the major axes of the nanorods, except Fb molecules, which have minor axis-1 aligned with the major axes of the nanorods. According to effective medium theory,[44] the effective refractive index of local dielectric medium in the gap region between the nanorods due to the presence of biomolecules can be expressed as $n_m = xn_p + (1 - x)n_b$, where n_p and n_b are the refractive indices of the protein molecule and the buffer medium, respectively, and x is the volume fraction of the protein molecule in the gap

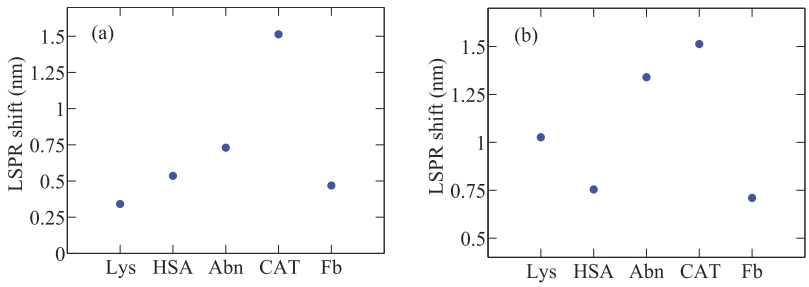

FIG. 13. (a) LSPR shifts for five protein molecules attached to the tips between the nanorods with a fixed gap width of 11 nm. (b) LSPR shifts for the protein molecules when the distance between the nanorods is optimized.

region. From Table I, we find that heavier biomolecules have larger physical dimensions, and hence, heavier molecules will have a greater volume fraction in the local environment. We find that the LSPR shift mainly depends on the change of n_m due to the presence of biomolecule between the tips of nanorods. Although Lys has the highest refractive index among the molecules considered in this work, it has the smallest size and mass. Therefore, a Lys molecule hardly changes n_m, and hence, shows the lowest LSPR shift of 0.3416 nm among the molecules considered in this work. Similarly, although Fb is the heaviest among the molecules, it has the lowest refractive index. Therefore, a Fb molecule also changes n_m by a small amount, and hence, shows a relatively small LSPR shift of 0.4684 nm. However, CAT molecules are heavy and they have a high refractive index as well. Therefore, a CAT molecule changes n_m significantly, and hence, shows an LSPR shift of 1.513 nm, which is the greatest among the biomolecules considered in this work.

In Fig. 13(b), we show the peak LSPR shifts for each protein molecule by optimizing the distance between the protein molecules and the tips of the nanorods. An optimized distance between the protein molecules and the tips of the nanorods increases n_m. Therefore, we find an increase in the LSPR shifts for all protein molecules. While Lys molecules show only an LSPR shift of 0.3416 nm for the case shown in Fig. 13(a), they show an LSPR shift of > 1 nm when the distance between the biomolecule and nanorods is optimized. Similarly, Fb molecules show a significant shift of 0.71 nm when the distance between the biomolecule and nanorods is optimized. We note that the LSPR shifts slightly depend on the orientation of the biomolecules with respect to the nanorods as the biomolecules are ellipsoid in shape. However, we find that the LSPR shifts due to the presence of a biomolecule is $\gtrsim$0.3 nm irrespective of the orientation of the biomolecules, which can be easily measured by modern detectors.

We find that an Au@Ag nanorod dimer sensor shows significant LSPR shifts in the presence of the biomolecules so that reliable detection of biomolecules is possible. Although a relatively greater LSPR shift does not provide additional information than the presence of a biomolecule, it represents a relatively higher sensitivity of the sensor, which is a desirable characteristic of any sensor system for reliable detection, especially against a noisy background. The greater LSPR shifts also reduce the requirement of a sophisticated detection system.

An Au@Ag nanorod dimer sensor will be selective to the target molecule by its choice of ligands. However, in practice, a sample may contain unwanted biomolecules in the background in addition to the target biomolecule. Intrinsically, the effect of the unwanted noise biomolecule in a nanorod dimer sensor will be less as the plasmonic resonance predominantly confines light between the tips of the nanorods, which is occupied by the target biomolecule. Nevertheless, it is important to study the impact of the noise background on an Au@Ag nanorod dimer sensor. We study the effect on LSPR shift when CAT molecules are detected in the presence of HSA noise molecules in the background. Both CAT and HSA are essential proteins in human blood plasma.[45,46] While the CAT molecule is attached to the tips of nanorods, the position of the HSA noise molecule will vary. We vary the position and distance of the HSA molecule with respect to the CAT molecule and calculate the change in LSPR shift with respect to when there is no noise molecule in the background. In Table III, we present the maximum percentage change in LSPR shift for varying position of the noise HSA molecule but at a fixed distance from the CAT molecule. We find the LSPR shift of CAT molecule changes by ~8.85% when HSA noise molecule is located too close to the CAT molecule at 1 nm.

TABLE III. % LSPR change due to noise biomolecules.

Target molecule	Noise molecule	Distance between target and noise molecules (nm)	% LSPR change
CAT	HSA	1	8.85
		2	6.77
		3	4.19
		4	0.73
CAT	Abn	1	11.8
		2	9.31
		3	5.63
		4	1.45

We find that the change in LSPR shift decreases to ~0.73% when the noise HSA molecule is located at 4 nm. We also calculated the change in LSPR shift when Abn molecules are present as the noise background. Abn molecules occur in human serum along with CAT molecules.[47,48] The LSPR shift changes by ~11.8% when noise Abn molecule is located at 1 nm with respect to the CAT molecule, which decreases to only ~1.45% when Abn molecule is located at 4 nm.

V. CONCLUSIONS

In conclusion, we studied the dynamics of Au@Ag nanorod dimers in detail both analytically and computationally. The results obtained using the developed analytical model match well with that obtained using FDTD simulations. Au@Ag nanorod dimers show enhanced sensitivity in label-free single molecule detection compared to that obtained from single Au@Ag nanorods or Au@Ag nanosphere dimers. Au@Ag nanorod dimers show greater absorption and coupling of the incident light due to the excitation of strong plasmonic modes when TM-polarized light is incident compared to that when TE-polarized light is incident. The sensitivity of Au@Ag nanorod dimers increases when Ag shell thickness increases, nanorods are aligned along the longitudinal axes, and the light is normally incident. Au@Ag nanorod dimers show significant sensitivity of ~0.3416–1.513 nm, i.e., shift in the LSPR wavelength, when single molecules of Lys, HSA, Abn, CAT, and Fb attach to the tips of the nanorods in the gap region. The sensitivity is not significantly affected when unwanted noise biomolecules are present in the background even only at a few nm from the target biomolecule.

[1] M. Grzelczak, J. Perez-Juste, P. Mulvaney, and L. M. Liz-Marzan, Chemical Society Reviews **37**, 1783–1791 (2008).
[2] S. Y. Lee, S. H. Kim, S. G. Jang, C. J. Heo, J. W. Shim, and S. M. Yang, Analytical Chemistry **83**, 9174–9180 (2011).
[3] M. Rycenga, C. M. Cobley, J. Zeng, W. Y. Li, C. H. Moran, Q. Zhang, D. Qin, and Y. N. Xia, Chemical Reviews **111**, 3669–3712 (2011).
[4] H. H. Wang, C. Y. Liu, S. B. Wu, N. W. Liu, C. Y. Peng, T. H. Chan, C. F. Hsu, J. K. Wang, and Y. L. Wang, Advanced Materials **18**, 491–495 (2006).
[5] R. F. Oulton, V. J. Sorger, D. A. Genov, D. F. P. Pile, and X. Zhang, Nature Photonics **2**, 496–500 (2008).
[6] K. M. Mayer and J. H. Hafner, Chemical Reviews **111**, 3828–3857 (2011).
[7] E. C. Dreaden, A. M. Alkilany, X. H. Huang, C. J. Murphy, and M. A. El-Sayed, Chemical Society Reviews **41**, 2740–2779 (2012).
[8] K. A. Willets and R. P. Van Duyne, Annual Review of Physical Chemistry **58**, 267–297 (2007).
[9] J. N. Anker, W. P. Hall, O. Lyandres, N. C. Shah, J. Zhao, and R. P. Van Duyne, Nature Materials **7**, 442–453 (2008).
[10] A. Jakab, C. Rosmen, Y. Khalavka, J. Becker, A. Trugler, U. Hohenester, and C. Sönnichsen, ACS Nano **5**, 6880–6885 (2011).
[11] Y. Li, W. Qi, B. Huang, W. Ji, and M. Wang, The Journal of Physical Chemistry C **117**, 15394–15401 (2013).
[12] Q. Fu, H. L. Liu, Z. Wu, A. Liu, C. Yao, X. Li, W. Xiao, S. Yu, Z. Luo, and Y. Tang, Journal of Nanobiotechnology **13**, 1–9 (2015).
[13] K. Liu, Y. Bai, L. Zhang, Z. Yang, Q. Fan, H. Zheng, Y. Yin, and C. Gao, Nano Letters **16**, 3675–3681 (2016).
[14] A. K. Samal, L. Polavarapu, S. R. Cedeira, L. M. L. Marzán, J. P. Juste, and I. P. Santos, Langmuir **29**, 15076–15082 (2013).
[15] M. S. Shore, J. Wang, A. C.J. Peck, A. L. Oldenburg, and J. B. Tracy, Small **7**, 230–234 (2011).
[16] L. Tang, S. Li, L. Xu, W. Ma, H. Kuang, L. Wang, and C. Xu, ACS Applied Materials & Interfaces **7**, 12708–12712 (2015).
[17] J. Cao, T. Sun, and K. T. V. Grattan, Sensors and Actuators B **195**, 332–351 (2014).
[18] P. Zijlstra, P. M. R. Paulo, and M. Orrit, Nature Nanotechnology **7**, 379–382 (2012).
[19] G. J. Nusz, A. C. Curry, S. M. Marinakos, A. Wax, and A. Chilkoti, ACS Nano **3**, 795–806 (2009).
[20] B. Willingham, D. W. Brandl, and P. Nordlander, Applied Physics B **93**, 209–216 (2008).
[21] J. Wu, X. Lu, Q. Zhu, J. Zhao, Q. Shen, L. Zhan, and W. Ni, Nano-Micro Letters **6**, 372–380 (2014).
[22] Y. Lu, Q. Yang, G. Du, F. Chen, Y. Wu, Y. Ou, J. Si, and X. Hou, Plasmonic **10**, 1325–1330 (2015).
[23] I. Torsteinsdóttir, L. Håkansson, R. Hällgren, B. Gudbjörnsson, N.-G. Arvidson, and P. Venge, Rheumatology **38**, 1249–1254 (1999).
[24] H. J. Lee, A. W. Wark, and R. M. Corn, Analyst **133**, 975–983 (2008).
[25] S. H. Kim, M. Fountoulakis, N. Cairns, and G. Lubec, *Protein Expression in Down Syndrome Brain* (Springer, 2013).
[26] H. P. Erickson, Biological Procedures Online **11**, 32–51 (2009).
[27] J. R. Colvin, Canadian Journal of Chemistry **30**, 831–834 (1952).
[28] J. Voros, Biophysical Journal **87**, 553–561 (2004).
[29] J. L. Felhofer, J. D. Caranto, and C. D. Garcia, Langmuir **26**, 17178–17183 (2010).
[30] https://www.thermofisher.com/uk/en/home/life-science/protein-biology/protein-biology- learning-center/protein-biology-resource-library/pierce-protein-methods/ overview-protein-labeling.html
[31] R. A. Weisiger, J. D. Ostrow, R. K. Koehler, C. C. Webster, P. Mukerjee, L. Pascolo, and C. Tiribelli, Journal of Biological Chemistry **276**, 29953–29960 (2001).
[32] J. S. Beckman, R. L. Minor, Jr., C. L. White, J. E. Repine, G. M. Rosen, and B. A. Freeman, The Journal of Biological Chemistry **263**, 6884–6892 (1988).
[33] H. M. Laborde, A. M. N. Lima, F. C. C. L. Loureiro, C. Thirstrup, and H. Neff, Thin Solid Films **540**, 221–226 (2013).

[34] S. R. Kudavelly and E. J. Meijer, US Patent 20130070230 A1 (2013).
[35] S. Ottani, D. Vitalini, F. Comelli, and C. Castellari, Journal of Chemical and Engineering Data **47**, 1197–1204 (2002).
[36] L. Shao, K. C. Woo, H. Chen, Z. Jin, J. Wang, and H.-Q. Lin, ACS Nano **4**, 3053–3062 (2010).
[37] N. G. Khlebtsov and B. N. Khlebtsov, Proceedings of SPIE: International Society for Optical Engineering **6164**, 1–14 (2006).
[38] R. Gans, Annalen der Physik **342**, 881–900 (1912).
[39] Q. Fu, D. G. Zhang, M. F. Yi, X. X. Wang, Y. K. Chen, P. Wang, and H. Ming, Journal of Optics **14**, 085001 (2012).
[40] M. Gluodenis and C. A. Foss, Journal of Physical Chemistry B **106**, 9484–9489 (2002).
[41] C. F. Bohren and D. R. Huffman, *Absorption and scattering of light by small particles* (Wiley, 1983).
[42] P. B. Johnson and R. W. Christy, Physical Review B **6**, 4370–4379 (1972).
[43] M. A. Awal, Z. Ahmed, and M. A. Talukder, Journal of Applied Physics **117**, 063109 (2015).
[44] W. Cai and V. Shalaev, *Optical Metamaterials Fundamentals and Applications* (Springer, 2010).
[45] D. D. Rutstein, E. F. Ingenito, W. E. Reynolds, and J. M. Burke, The Journal of Clinical Investigation **33**, 211–221 (1954).
[46] B. Frei, Y. Yamamoto, D. Niclas, and B. N. Ames, Analytical Biochemistry **175**, 120–130 (1988).
[47] G. L. Dale, P. Gaddy, and F. J. Piklu, The Journal of Laboratory and Clinical Medicine **123**, 365–371 (1994).
[48] J. A. Leff, M. A. Oppegard, L. S. Terada, E. C. McCarty, and J. E. Repine, Journal of Applied Physiology **71**, 1903–1906 (1991).